Biosensors and Bioelectronics 42 (2013) 293–299

Contents lists available at SciVerse ScienceDirect

Biosensors and Bioelectronics

journal homepage: www.elsevier.com/locate/bios

Facile preparation of novel core–shell enzyme–Au–polydopamine–Fe_3O_4 magnetic bionanoparticles for glucose sensor

Hua-Ping Peng [a,b], Ru-Ping Liang [a,*], Li Zhang [a], Jian-Ding Qiu [a,*]

[a] Department of Chemistry, Nanchang University, Nanchang 330031, China
[b] Faculty of Pharmacy, Fujian Medical University, Fuzhou 350004, China

ARTICLE INFO

Article history:
Received 25 July 2012
Received in revised form
23 October 2012
Accepted 24 October 2012
Available online 8 November 2012

Keywords:
Dopamine
Magnetic nanoparticles
Au nanoparticles
Glucose oxidase
Direct electrochemistry
Biosensor

ABSTRACT

In this study, a novel biomolecule immobilization approach has been proposed to the synthesis of multi-functional core–shell glucose oxidase–Au–polydopamine–Fe_3O_4 magnetic bionanoparticles (GOx–Au–PDA–Fe_3O_4 MBNPs) using the one-pot chemical polymerization method. Then, a high performance biosensor has been constructed by effectively attaching the proposed GOx–Au–PDA–Fe_3O_4 MBNPs to the surface of the magnetic glassy carbon electrode. Scanning electron microscope, energy dispersive x-ray spectrometer, UV–vis spectroscopy, and electrochemical methods were used to characterize the GOx–Au–PDA–Fe_3O_4 MBNPs. The resultant GOx–Au–PDA–Fe_3O_4 MBNPs not only have the magnetism of Fe_3O_4 nanoparticles which makes them easily manipulated by an external magnetic field, but also have the excellent biocompatibility of PDA to maintain the native structure of the GOx, and good conductivity of Au nanoparticles which can facilitate the direct electrochemistry of GOx in the biofilm. Hence, the present GOx–Au–PDA–Fe_3O_4 biofilm displays good linear amperometric response to glucose concentration ranging from 0.02 to 1.875 mM. This efficient biomolecule immobilization platform is recommended for the preparation of many other MBNPs with interesting properties and application potentials in many fields, such as biosensing, biocatalysis, biofuel cells, and bioaffinity separation.

1. Introduction

The studies of direct electrochemistry of redox proteins/enzymes at electrodes are of scientific importance in the investigation of the fundamental mechanism of biological redox reactions and of practical significance for the development of advanced bioelectronic devices, such as highly sensitive enzymatic biosensors and highly efficient biofuel cells (Ivnitski et al., 2008; Elliott et al., 2009; Wang et al., 2009; Yan et al., 2006). Nevertheless, establishment of direct electron transfer between immobilized flavoprotein oxidase systems such as glucose oxidase (GOx) and conventional electrodes is extremely difficult because of the inaccessibility of the active centers. The reasons could be due to the fact that the active center is deeply embedded in a thick insulating protein shell, and/or occurrence of denaturation of the adsorbed proteins which results in passivation of the electrode surfaces (Cai and Chen, 2004; Wang and Yuan, 2003; Wilson and Turner, 1992). Many attempts using casting (Guo and Li, 2010), self-assembly (Shan et al., 2009), entrapping (Wang et al., 2009), sol–gel (Nadzhafova et al., 2007), layer by layer (Deng et al., 2010), covalent binding (Liu et al., 2010), and various inorganic/organic substances such as graphene (Shan et al., 2009), conducting polymer nanowires (Hong et al., 2009), nano-metal oxides (Guo and Li, 2010) have been made to improve the electron communication between the active site of GOx and electrode. Although direct electrochemistry could be achieved on the modified electrodes, only a few examples of reversible electrochemical behavior of the immobilized GOx have been observed. In addition, the bioactivity of the enzyme may be weakened or even disappeared during the immobilization procedure. Thus, development of a simple procedure which enables the stability of the immobilized GOx with natural conformation to achieve enhanced direct electrochemistry of GOx remains challenges.

Recently, inspired by the adhesive proteins of mussle, Messersmith and colleagues developed a simple but versatile surface modification approach in which self-polymerization of dopamine at weak alkaline pH produced an adherent polydopamine (PDA) coating on a wide variety of materials (Lee et al., 2007). The derived films can further support a variety of secondary reactions and create various functional PDA films. This approach is simple, inexpensive, quick, and "green" (Lee et al., 2007, 2008; Yang et al., 2011; Zhang et al., 2010, 2012). In addition, due to the good chemical stability, excellent hydrophilic and biocompatible

* Corresponding author. Tel.: +86 791 83969518.
E-mail addresses: liangrp@163.com (R.-P. Liang), jdqiu@ncu.edu.cn (J.-D. Qiu).

0956-5663/$ - see front matter © 2012 Elsevier B.V. All rights reserved.
http://dx.doi.org/10.1016/j.bios.2012.10.074

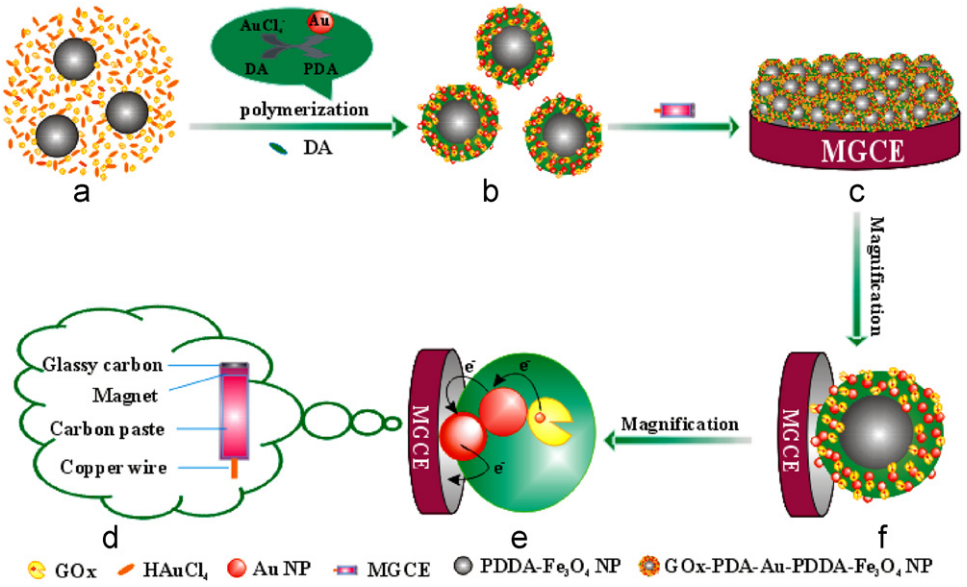

Scheme 1. Schematic illustration of the procedure for preparation of GOx–PDA–Au–Fe_3O_4 MBNPs film modified magnetic glassy carbon electrode.

properties of PDA, the design and synthesis of multi-functional PDA-based bio-nanocomposites with interesting properties has been proven to be an efficient approach for the construction of high performance biosensing (Fu et al., 2009, 2010a; Tan et al., 2010; Wang et al., 2011). For example, Fu and co-workers have prepared Au nanoparticles (NPs)/PDA–Pt NPs–GOx bionanocomposites with PDA as an efficient matrix to support antibody for sandwich-type amperometric immunoassay (Fu et al., 2010b). Tan et al. have reported the facile preparation of PDA–enzyme–multi-walled carbon nanotube cast films for electrochemical biosensing and biofuel cell applications (Tan et al., 2010).

Herein, multi-functional core–shell GOx–PDA–Au–Fe_3O_4 MBNPs were synthesized by a simple one-pot in situ chemical polymerization method. As shown in Scheme 1, dopamine was added dropwise to the aqueous mixture of GOx, $HAuCl_4$ and PDDA–Fe_3O_4 NPs (Scheme 1a). Due to the in situ chemical polymerization of dopamine by $HAuCl_4$ in the mixture, core–shell enzyme–PDA–Au–Fe_3O_4 MBNPs was successfully prepared (Scheme 1b). And then, with the advantages of the magnetism of the MBNPs, the proposed MBNPs were effectively deposited on the electrode surface by applying a constant magnetic field (Scheme 1c), thus a high performance glucose sensor has been constructed using the GOx–Au–PDA–Fe_3O_4 MBNPs. The morphology, structure, and electrochemistry of the MBNPs were characterized by scanning electron microscope, energy dispersive x-ray spectrometer, UV–vis spectroscopy, and electrochemical methods respectively. The modified electrode based on this GOx–PDA–Au–Fe_3O_4 MBNPs film well retained the native structure of the immobilized protein, successfully realized the direct electron transfer of the immobilized GOx and displayed good electrocatalytic activity to the oxidation of glucose. The proposed method is highly recommended as a new biosensing platform for biomolecule immobilizations and biocatalysis applications.

2. Materials and methods

2.1. Materials

Glucose oxidase (GOx, EC 1.1.3.4; type II from Aspergillus niger, 150 KU g^{-1}) and poly(diallyldimethylammonium chloride) (PDDA) were purchased from Sigma. Dopamine was purchased from Alfa Aesar. All other chemicals, such as glucose and $HAuCl_4 \cdot 4H_2O$ were of analytical grade and used as received. A permanent magnet was purchased from As One Ltd. (Osaka, Japan). 0.1 M phosphate buffer saline (PBS, pH 6.98) was used as supporting electrolyte. All solutions were prepared with doubly distilled water.

2.2. Synthesis of Fe_3O_4 NPs

The Fe_3O_4 NPs were prepared through a solvothermal reaction according to Deng et al. 2005. Briefly, $FeCl_3 \cdot 6H_2O$ (1.35 g) and sodium acetate (3.60 g) were dissolved in 50 mL of ethylene glycol under magnetic stirring. After the well-proportioned mixtures were dispersed, the yellow solution was transferred to a Teflon-lined stainless-steel autoclave and sealed to heat at 200 °C. After reaction for 8 h, the autoclave was cooled to room temperature. The obtained black magnetite particles were washed with ethanol for several times. Finally the products were collected with a magnet, and then dried under vacuum at room temperature.

2.3. Synthesis of PDDA–Fe_3O_4 NPs

The PDDA–Fe_3O_4 NPs were prepared according to the literature with some modification (Fang et al., 2010). A 3 mL portion of 1 mg mL^{-1} Fe_3O_4 NPs was dispersed in 12 mL of aqueous solution containing 0.625 M potassium chloride (KCl) and 1.25 mg mL^{-1} PDDA. After being mixed well, the mixture was sonicated for 3 h. Excess PDDA was removed by separation with a magnet and rinsed with water for several times. Finally the PDDA–Fe_3O_4 NPs were redispersed in 6 mL of water.

2.4. Synthesis of GOx–PDA–Au–Fe_3O_4 MBNPs

The GOx–PDA–Au–Fe_3O_4 MBNPs were prepared as follows. 300 μL of 2% $HAuCl_4$ and 5.0 mg GOx were added to 1.0 mL PBS containing 0.5 mg mL^{-1} PDDA–Fe_3O_4 NPs under vigorous stirring at 4 °C. Then, 500 μL of 60 mM (excess) dopamine was added dropwise to the mixture, the reaction mixture was stirred to allow a complete reaction for 20 min to form GOx–PDA–Au–Fe_3O_4 MBNPs. After reaction, the product was collected with a magnet and washed with water for several times, finally suspended in 1 mL PBS (pH 6.98) and stored at 4 °C when not used.

2.5. Electrode preparation

The magnetic glassy carbon electrode (MGCE) was prepared according to our previous method (Qiu et al., 2010). Briefly, paraffin oil (1.2 mL) was mixed with graphite powder (10 mg) thoroughly to get homogeneous paste. A copper wire was put into a Teflon tube (3 mm in diameter and 50 mm in depth) which was initially filled with a portion of the resulting paste, and a nummular magnet (3 mm in diameter and 2 mm in thickness, 0.2 T at the surface) was embedded with a depth of 2 mm from the surface of electrode. Then a glassy carbon (3 mm in diameter and 2 mm in depth) was inserted in the tube to immobilize the magnet and the edge of the glassy carbon was sealed by the adhesive. After carefully polishing with 1.0, 0.3 and 0.05 μm alumina slurry successively and then ultrasonicating in water for a few minutes, 10 μL of the GOx–PDA–Au–Fe_3O_4 MBNPs solution was dripped onto the bare MGCE, the solid GOx–PDA–Au–Fe_3O_4 MBNPs were firmly attached to the electrode surface with the help of magnetic force. After drying for 1 h, the electrode surface was washed with PBS. When not in use, the modified electrode was stored in a moist state at 4 °C.

2.6. Characterization

Electrochemical experiments were performed on an Autolab PGSTAT30 electrochemical workstation (Eco Chemie). A three-electrode system was used with a saturated calomel electrode (SCE) as the reference electrode, a platinum wire as the auxiliary electrode, and the modified MGCE as the working electrode. The electrolyte solutions were purged with N_2 for at least 20 min to remove O_2 and kept under N_2 atmosphere during measurements. Scanning electron microscopy (SEM) images were collected on a Quanta 200F scanning electron microscope (FEI, USA). The transmission electron microscope (TEM) was performed on JEOL 2010 transmission electron microscopy operated at an accelerating voltage of 200 kV. To analyze the elements of GOx–PDA–Au–Fe_3O_4 MBNPs, energy dispersive X-ray (EDS) analysis was also carried out. UV–vis absorption spectra were acquired with a UV-2450 spectrophotometer (Shimadzu).

3. Results and discussion

3.1. Preparation and characterization of the GOx–PDA–Au–Fe_3O_4/MGCE

As illustrated in Scheme 1, GOx, $HAuCl_4$ and PDDA–Fe_3O_4 NPs were dissolved in a pH 6.98 PBS (Scheme 1a), and then dopamine was added dropwise to yield Au NPs and PDA. In this experiment, dopamine as a reductant and a monomer was oxidized to PDA by the $HAuCl_4$, resulting in the formation of PDA and Au NPs. Due to the in situ chemical polymerization of dopamine triggered by oxidizing reagent $HAuCl_4$ in the mixture, core–shell enzyme–PDA–Au–Fe_3O_4 MBNPs was successfully prepared (Scheme 1b). SEM and TEM images were used to confirm the formation and observe the morphologies of the GOx–PDA–Au coating deposited on the Fe_3O_4 surface (Fig. 1). As can be seen from the SEM images, both the Fe_3O_4 NPs and GOx–PDA–Au–Fe_3O_4 MBNPs are monodispersed and have uniformed size (Fig. 1A and B). The Fe_3O_4 NPs with a diameter of 160–180 nm show rough surface morphology (Fig. 1A). After the in situ polymerization reaction, many densely dispersed Au NPs are homogeneously produced inside and outside the PDA film without aggregation, and the diameter of the GOx–PDA–Au–Fe_3O_4 MBNPs increased by ~25 nm (Fig. 1B). As can be seen from TEM image, the Fe_3O_4 NPs are an assembly of

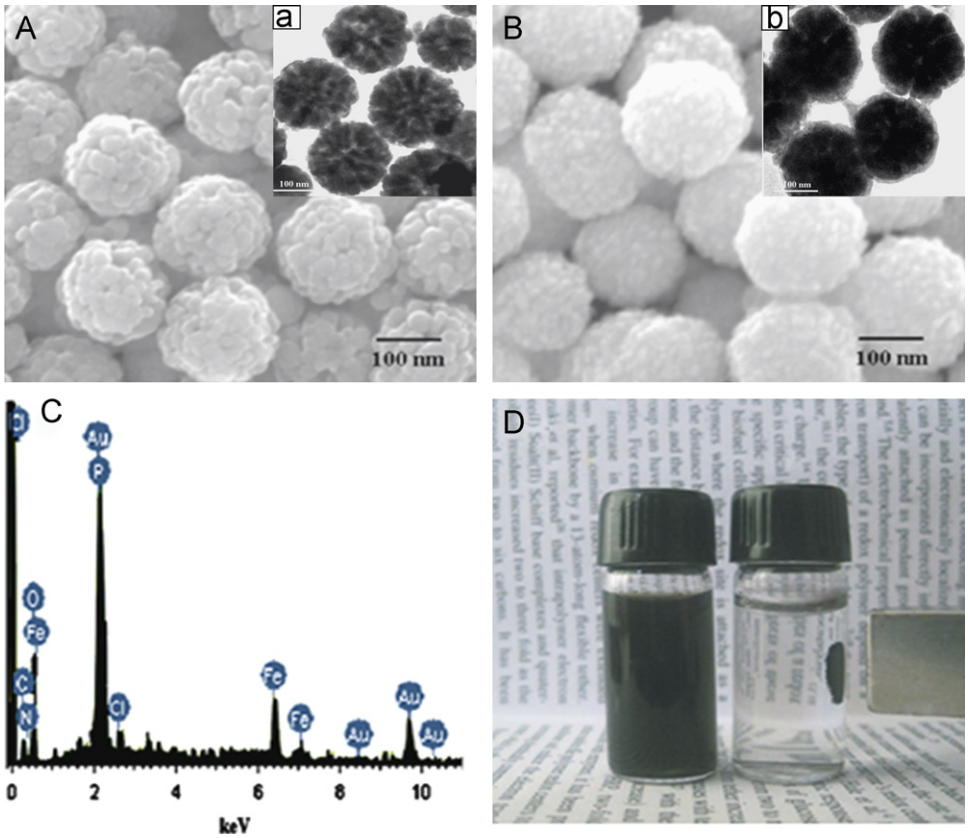

Fig. 1. SEM (A, B) and TEM (a, b) images of Fe_3O_4 NPs and GOx–PDA–Au–Fe_3O_4 MBNPs. (C) The EDS spectrum of the GOx–PDA–Au–Fe_3O_4 MBNPs. (D) Photograph of the GOx–PDA–Au–Fe_3O_4 MBNPs in absence (left) and presence (right) of external magnetic field.

many small Fe_3O_4 nanocrystals (Deng et al., 2005) and these particles are spherical and remarkably uniform and well dispersed in aqueous solution (Fig. 1a). After formation of GOx–PDA–Au–Fe_3O_4 MBNPs with well-defined core–shell structures through in situ polymerization reaction, the TEM image shows that all the Fe_3O_4 cores (dark) are wrapped by the composite PDA (gray) coating layer (Zhou et al., 2010), and there are many Au NPs homogeneously decorating on/in the MBNPs (Fig. 1b). Thus, we can speculate that the GOx molecules would be immobilized both on the surface and in the porous structures of the Fe_3O_4 NPs, which greatly increase the loading of the GOx and no obvious changes in size or shape of the Fe_3O_4 cores are observed. The energy dispersive x-ray spectrometer (EDS) measurement of the MBNPs reveals the existence of C, N, O, Fe, P, Cl and Au elements (Fig. 1C), confirming the successful formation of the core–shell GOx–PDA–Au–Fe_3O_4 MBNPs by the present one-pot in situ polymerization approach. As shown in Fig. 1D, the GOx–PDA–Au–Fe_3O_4 MBNPs suspension is homogeneous and black. Once an external magnetic field is applied, the GOx–PDA–Au–Fe_3O_4 MBNPs are attracted immediately toward the magnet, leaving the bulk solution clear and transparent. These results demonstrate that with the advantage of the inherent magnetic property of the Fe_3O_4 NPs, the prepared GOx–PDA–Au–Fe_3O_4 MBNPs can be simply assembled on a MGCE by applying a constant magnetic field, thus fabricating a high performance glucose biosensor (Scheme 1c). In the presented system, GOx with remaining bioactivity can be efficiently trapped in the formed matrix at high load and due to the gentle in situ polymerization process of dopamine and the excellent biocompatible microenvironment provided by the PDA and Au NPs. The entrapped GOx molecules are stable due to the excellent adhensive property of the as-formed PDA (Lee et al., 2007). Furthermore, the positive charged PDDA shell over the magnetic NPs prevents the agglomeration of the mixture, and the magnetic properties of the MBNPs make them easily manipulated by an external magnetic field. Compared with the conventional methods, this method greatly simplifies the biomolecule immobilization methodology and well retains its bioactivity due to the inherent magnetism of Fe_3O_4, the excellent biocompatibility of PDA, the absence of other special agents and no complex immobilization process. Besides, due to the good conductivity of the Au NPs in MBNPs, enhanced electron communication between GOx and electrode can be achieved (Scheme 1e).

3.2. UV–vis spectroscopy

UV–vis spectroscopy has been employed to monitor the formation of GOx–PDA–Au–Fe_3O_4 MBNPs and study the effects of the MBNPs on the microstructures of GOx. As shown in Fig. 2, in the case of PDDA–Fe_3O_4, no obvious absorption peak is observed (curve a). The GOx solution exhibits an intense band at 278 nm and two well-defined peaks of light absorption at 375 and 450 nm (curve b), which is in agreement with the result in literature (Zhao et al., 2006). The above peaks can also be observed in the GOx–PDA–Au–Fe_3O_4 MBNPs solution and nearly have no difference in the site (curve c), indicating the GOx keeps its natural structure in the GOx–PDA–Au–Fe_3O_4 MBNPs. Besides, a novel absorption peaks occurred at 560 nm is observed which due to the absorption of the nanosized Au NPs in MBNPs. Thus, the UV–vis absorbance spectrum further confirms the formation of Au NPs by this simple one-pot in situ chemical polymerization method, and the entrapped GOx in the GOx–PDA–Au–Fe_3O_4 MBNPs retains its native structure. This result may be explained as follows. The GOx–PDA–Au–Fe_3O_4 MBNPs provide a biocompatible microenvironment by the PDA and Au NPs to preserve the biological activity of the immobilized biomolecule. Furthermore, the MBNPs are formed in situ in the suspension, and the solution-state

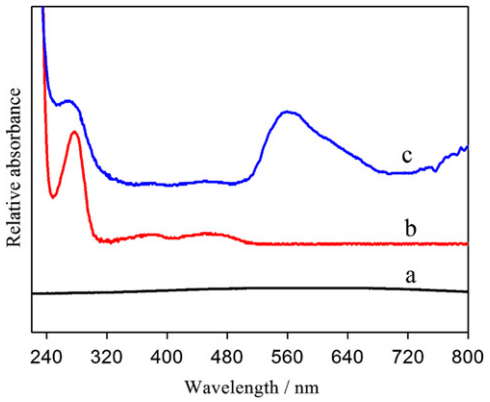

Fig. 2. UV–vis spectra of PDDA–Fe_3O_4 (a) GOx (b) GOx–PDA–Au–Fe_3O_4 (c) solutions.

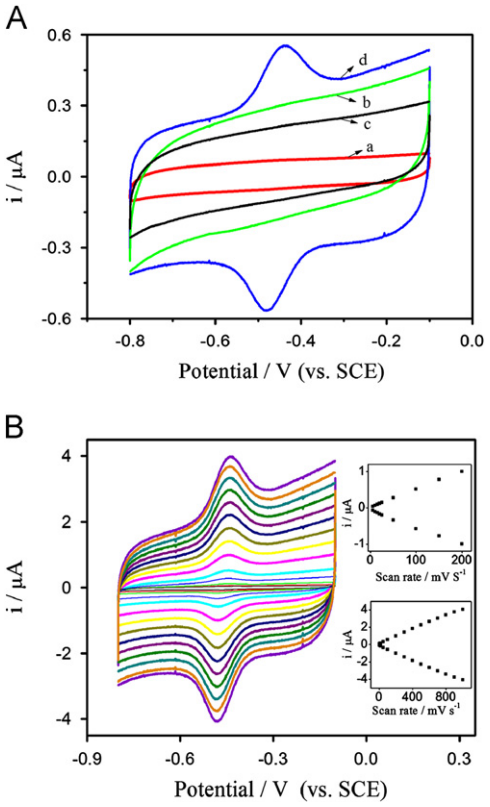

Fig. 3. (A) CVs of GOx (a), PDA–Au–Fe_3O_4 (b), bare (c), GOx–PDA–Au–Fe_3O_4 (d) modified electrodes in 0.1 M pH 6.98 PBS at a scan rate of 100 mV s^{-1}. (B) CVs of the GOx–PDA–Au–Fe_3O_4/MGCE in PBS (pH 6.98) at different scan rates. Scan rate (from internal to external) is 5, 10, 20, 50, 100, 200, 300, 400, 500, 600, 700, 800, 900 and 1000 mV s^{-1}. Inset: Plots of the anodic and cathodic peak currents as function of scan rate. In all these measurements, dissolved oxygen in solution was removed by bubbling nitrogen for 20 min.

protein molecules of high conformational freedom may be more adaptable to the in situ enwrapping. Thus, the biomolecules suffer little from distortion in conformation and its bioactivity can be more effectively retained in the composites (Fu et al., 2008).

3.3. Direct electrochemistry and electrocatalytic activity of the GOx–PDA–Au–Fe_3O_4/MGCE

Fig. 3A shows the cyclic voltammograms (CVs) in 0.1 M pH 6.98 PBS. As expected, the GOx-modified MGCE does not show discernible redox peaks (curve a), indicating that direct electrochemistry of the immobilized GOx does not occur due to the

inaccessibility of the active site, unfavorable orientation and/or the denaturation of the protein molecules at the bare MGCE surface. The PDA–Au–Fe_3O_4/MGCE only shows an increased background curve (curve b) as compared to the bare electrode (curve c) due to the three-dimensional matrix of the PDA–Au–Fe_3O_4 film. For the GOx–PDA–Au–Fe_3O_4/MGCE, a pair of well-defined redox peaks at −436 and −480 mV appears, showing the characteristics of reversible electron transfer process of redox active center (flavin adenine dinucleotide, FAD) in GOx (curve d) (Shan et al., 2009). The formal potential of GOx is −458 mV, which is very close to the standard electrode potential of −460 mV (vs. a saturated calomel electrode) for FAD/$FADH_2$ at pH 7.0 (25 °C) (Wu et al., 2007), indicating that the entrapped GOx molecules retain their native structure in the GOx–PDA–Au–Fe_3O_4 film. The good electrochemical response of GOx may be mainly due to penetration of the Au NPs in MBNPs to the active center of GOx which greatly shortens the electron tunneling path. The anodic and cathodic peak currents increase linearly with the scan rates (Fig. 3B), which suggests that direct electron transfer reaction of GOx is a surface-controlled process (Guo et al., 2011).

Since $n\Delta E_p < 200$ mV (E_p: peak potential), the direct electron-transfer rate constant (K_s) of the immobilized GOx on the GOx–Au–PDA–Fe_3O_4/MGCE can be obtained by Eq. (1) (Laviron 1979),

$$\log K_s = \alpha \log(1-\alpha) + (1-\alpha)\log\alpha - \log\frac{RT}{nF\nu} - \alpha(1-\alpha)\frac{nF\Delta E_p}{2.3RT} \quad (1)$$

where α is the charge-transfer coefficient, ΔE_p is the peak potential separation, ν is the scan rate, n is the number of electron transferred, and F is Faraday's constant. Our experimental results show that the scan rate in the range of $5-1000$ mV s^{-1} did not affect the K_s value. Taking the charge-transfer coefficient α of 0.5, at a scan rate of 100 mV s^{-1}, the K_s of the immobilized GOx on the GOx–Au–PDA–Fe_3O_4/MGCE is calculated to be 3.8 s^{-1}. The value is much larger than those ever reported ones (Kang et al., 2009; Yang et al., 2008), indicating that the enhanced direct electron transfer of the GOx–PDA–Au–Fe_3O_4 biofilm. According to the Laviron eq. (2) (Laviron, 1979),

$$I_p = \frac{n^2F^2A\nu\Gamma}{4RT} = \frac{nFQ\nu}{4RT} \quad (2)$$

where Γ (mol cm^{-2}) is the surface amount of the adsorbed protein on electrode surface, A is the electrode area (cm^2), ν is the scan rate, I_p is the peak current, n is the number of electron transferred, Q is the charge involved in the reaction, and F is Faraday's constant. The average surface amount (Γ) of the immobilized GOx on the GOx–PDA–Au-Fe_3O_4/MGCE is estimated to be 8.4×10^{-11} mol cm^{-2}, which is 29.3 times larger than that (2.86×10^{-12} mol cm^{-2}) at the bare GCE (Liu and Ju, 2003). The increased functional density of GOx molecules can be attributed to the three-dimensional matrix of the GOx–PDA–Au–Fe_3O_4/MGCE. Another possibility is that the chemical oxidation polymerization can result in the high-load immobilization of the enzyme (Fu et al., 2008).

It is well known that the direct electrochemistry of GOx is a two-electron coupled with a two-proton reaction. Therefore, the solution pH should influence the electrochemical behavior of the immobilized GOx on GOx–PDA–Au–Fe_3O_4/MGCE. Fig. 4 shows the CVs of the GOx–PDA–Au–Fe_3O_4/MGCE in the PBS solutions with different pH values in the absence of oxygen. With the increase of solution pH from 4.0 to 9.0, a negative shift of both cathodic and anodic peak potentials is observed due to the proton transfer from FAD to the reduced $FADH_2$ ($FAD+2H^++2e^- \rightleftharpoons FADH_2$). In addition, all changes in the peak potentials and currents with solution pH are reversible. Furthermore, it is found that the formal potential of the GOx–PDA–Au–Fe_3O_4/MGCE decreases linearly

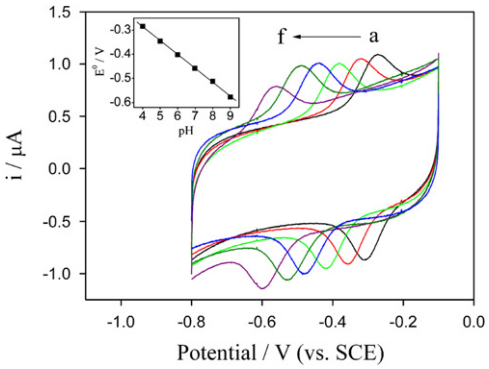

Fig. 4. CVs of GOx–PDA–Au–Fe_3O_4/MGCE in PBS with pH values of 4.0 (a), 5.0 (b), 6.0 (c), 6.98 (d), 8.0 (e), and 9.0 (f) at a scan rate of 200 mV s^{-1}. Inset: Plot of formal potential vs. pH.

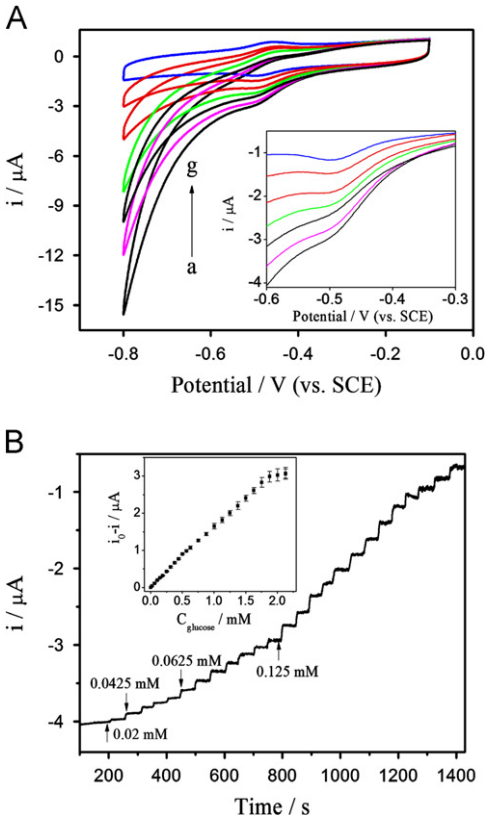

Fig. 5. (A) CVs of GOx–PDA–Au–Fe_3O_4/MGCE in oxygen-saturated 0.1 M pH 6.98 PBS containing 0 (a) 0.1 (b) 0.3 (c) 0.42 (d) 0.58 (e) 0.9 (f) and 1.1 mM (g) glucose at 200 mV s^{-1}. Inset: The enlarged curves from −0.6 V to −0.3 V. (B) Amperometric responses of GOx–PDA–Au–Fe_3O_4/MGCE at −0.5 V to successive addition of glucose in a stirred 0.1 M PBS (pH 6.98). Inset: Plot of the cathodic current as a function of glucose concentration.

with the pH in the range of 4.0–9.0 with a slop of −57.7 mV pH^{-1} (inset in Fig. 4), which is close to the expected value of −58.6 mV pH^{-1}, indicating a two-proton reaction coupled with a two-electron transfer process (Liu and Ju, 2003).

The immobilized GOx in the PDA–Au–Fe_3O_4 shows excellent bioactivity. As shown in Fig. 5A, addition of glucose to the PBS results in the decrease of reduction current at negative potentials originating from reduction of O_2. The decreased cathodic current decreases with the increase of glucose concentration because of the consumption of O_2. Based on this phenomenon, the concentration of glucose can be determined. Fig. 5B illustrates the amperometric response of the biosensor at −0.5 V to successive

addition of glucose. The present biosensor displays good linear amperometric response to glucose concentration ranging from 0.02 to 1.875 mM with a detection limit of 6.5 μM at signal to noise ratio of 3 (Fig. 5B, inset). When glucose concentration is high, the curvature from the initial straight line shows the characteristics of Michaelis–Menten kinetics. The apparent Michaelis–Menten constant (K_m^{app}), an important parameter to reveal enzyme-substrate reaction kinetics, can be calculated by the electrochemical version of the Lineweaver–Burk Eq. (3) (Kamin and Wilson, 1980):

$$\frac{1}{I_{ss}} = \frac{K_m^{app}}{I_{max}}\frac{1}{C} + \frac{1}{I_{max}} \quad (3)$$

here, I_{ss} is the steady state current after the addition of substrate, C is the bulk concentration of the substrate, and I_{max} is the maximum current measured under saturated substrate conditions. The K_m^{app} value for the enzymatic activity of the GOx–Au–PDA–Fe_3O_4/MGCE to glucose is calculated to be 1.67 mM, which is smaller than those reported for GOx immobilized on highly ordered polyaniline nanotubes (2.37 mM), GOx entrapped in polypyrrole films (19 mM), and GOx in Nafion film (14.91 mM) (Wang et al., 2009; Mousty et al., 2001; Ozoemena and NyoKong, 2006). The smaller value of K_m^{app} validates that the immobilized GOx in GOx–PDA–Au–Fe_3O_4 MBNPs possesses higher enzymatic activity.

3.4. Interference study

The effect of possible interfering species such as uric acid (UA), ascorbic acid (AA) and glycine on glucose detection has been examined. The electrochemical responses of 0.01 mM UA, AA or glycine in the absence of glucose are essentially negligible, and no significant interference is observed upon addition of 0.01 mM UA, AA or glycine in 0.1 mM glucose. These results suggest that the proposed GOx–PDA–Au–Fe_3O_4/MGCE has high selectivity, and no interference from coexisted electroactive substances due to the low operating potential.

3.5. Reproducibility and stability of the biosensor

The reproducibility of the proposed biosensor has been examined as well. The relative standard deviation (RSD) of the biosensor response to 1.0 mM glucose is 4.1% for 8 successive measurements. The RSD for detection of 1.0 mM glucose with five sensors prepared under the same conditions is 5.6%. The enzyme electrode is stored at 4 °C when not in use. It can retain 95% of its initial amperometric response after storage for 4 weeks. The excellent reproducibility and stability of the biosensor may be mainly attributed to the good biocompatibility of the MBNPs and the enzyme immobilization approach preventing leakage of biomolecules.

3.6. Determination of glucose in serum samples

To illustrate feasibility of the glucose sensor as a fundamental application, glucose concentration in human serum sample has been measured. An appropriate dilution of the sample with the supporting electrolyte before measurement is performed. Five parallel determinations are carried out. The glucose level is determined to be 5.56 mM close to the 5.46 mM determined by spectrophotometry, showing a good accuracy. The recoveries for the assays of 0.10–0.80 mM glucose are between 93% and 106% for eight measurements. The results are satisfactory and agree closely with those detected by the automated standard colorimetric technique in the hospital.

4. Conclusions

In summary, a simple biomolecule immobilization approach has been proposed to the synthesis of multi-functional GOx–PDA–Au–Fe_3O_4 core–shell MBNPs using a facile one-pot in situ chemical polymerization. The GOx–PDA–Au–Fe_3O_4 core–shell MBNPs retain magnetic response property and thus a GOx–PDA–Au–Fe_3O_4 core–shell MBNPs modified electrode can be easily prepared. The entrapped GOx retains its bioactivity due to the excellent biocompatibility of PDA and can communicate electrons with the electrode efficiently due to the electron rely function of gold nanoparticles. This work not only provides a versatile platform for biomolecule immobilization, but also provides a new insight into the preparation of many other magnetic bionanocomposites with interesting properties for potential applications in fields, such as molecularly imprinted polymers, drug delivery, biosensing, biocatalysis, biofuel cells, and bioaffinity separation.

Acknowledgment

This research was financially supported by the National Natural Science Foundation of China (21065006 and 21163014), the Program for New Century Excellent Talents in University (NCET-11–1002), the Program for Young Scientists of Jiangxi Province (20112BCB23001), and the Scientific Research Foundation for Doctoral Program of Fujian Medical University (2011BS005).

References

Cai, C., Chen, J., 2004. Analytical Biochemistry 332, 75–83.
Deng, C.Y., Chen, J.H., Nie, Z., Si, S.H., 2010. Biosensors and Bioelectronics 26, 213–219.
Deng, H., Li, X.L., Peng, Q., Wang, X., Chen, J.P., Li, Y.D., 2005. Angewandte Chemie—International Edition 44, 2782–2785.
Elliott, K.J., Harriman, A., Le Pleux, L., Pellegrin, Y., Blart, E., Mayer, C.R., Odobel, F., 2009. Physical Chemistry Chemical Physics 11, 8767–8773.
Fang, Y.X., Guo, S.J., Zhu, C.Z., Zhai, Y.M., Wang, E.K., 2010. Langmuir 26, 11277–11282.
Fu, Y., Chen, C., Xie, Q., Xu, X., Zou, C., Zhou, Q., Tan, L., Tang, H., Zhang, Y., Yao, S., 2008. Analytical Chemistry 80, 5829–5838.
Fu, Y.C., Li, P.H., Bu, L.J., Wang, T., Xie, Q.J., Xu, X.H., Lei, L.H., Zou, C., Yao, S.Z., 2010b. Journal of Physical Chemistry C 114, 1472–1480.
Fu, Y.C., Li, P.H., Wang, T., Bu, L.J., Xie, Q.J., Xu, X.H., Lei, L.H., Zou, C., Chen, J.H., Yao, S.Z., 2010a. Biosensors and Bioelectronics 25, 1699–1704.
Fu, Y.C., Li, P.H., Xie, Q.J., Xu, X.H., Lei, L.H., Chen, C., Zou, C., Deng, W.F., Yao, S.Z., 2009. Advanced Functional Materials 19, 1784–1791.
Guo, C.X., Li, C.M., 2010. Physical Chemistry Chemical Physics 12, 12153–12159.
Guo, C.X., Zheng, X.T., Ng, S.R., Lai, Y., Lei, Y., Li, C.M., 2011. Chemical Communications 47, 2652–2654.
Hong, Y.Y., Hsu, Y.K., Ganguly, A., Chen, C.C., Chen, L.C., Chen, K.H., 2009. Electrochemistry Communications 11, 850–853.
Ivnitski, D., Artyushkova, K., Rincon, R.A., Atanassov, P., Luckarift, H.R., Johnson, G.R., 2008. Small 4, 357–364.
Kamin, R.A., Wilson, G.S., 1980. Analytical Chemistry 52, 1198–1205.
Kang, X.H., Wang, J., Wu, H., Aksay, I.A., Liu, J., Lin, Y.H., 2009. Biosensors and Bioelectronics 25, 901–905.
Laviron, E., 1979. Journal of Electroanalytical Chemistry 100, 263–270.
Lee, H., Dellatore, S.M., Miller, W.M., Messersmith, P.B., 2007. Science 318, 426–430.
Lee, H., Rho, J., Messersmith, P.B., 2008. Advanced Materials 20, 1–4.
Liu, S., Ju, H.X., 2003. Biosensors and Bioelectronics 19, 177–183.
Liu, Y., Yu, D.S., Zeng, C., Miao, Z.C., Dai, L.M., 2010. Langmuir 26, 6158–6160.
Mousty, C., Galland, B., Cosnier, S., 2001. Electroanalysis 13, 186–190.
Nadzhafova, O., Etienne, M., Walcarius, A., 2007. Electrochemistry Communications 9, 1189–1195.
Ozoemena, K.I., Nyokong, T., 2006. Electrochimica Acta 51, 5131–5136.
Qiu, J.D., Peng, H.P., Liang, R.P., Xia, X.H., 2010. Biosensors and Bioelectronics 25, 1447–1453.
Shan, C.S., Yang, H.F., Song, J.F., Han, D.X., Ivaska, A., Niu, L., 2009. Analytical Chemistry 81, 2378–2382.
Tan, Y.M., Deng, W.F., Li, Y.Y., Huang, Z., Meng, Y., Xie, Q.J., Ma, M., Yao, S.Z., 2010. Journal of Physical Chemistry B 114, 5016–5024.
Wang, G.F., Huang, H., Zhang, G., Zhang, X.J., Fang, B., Wang, L., 2011. Langmuir 27, 1224–1231.

Wang, L., Yuan, Z., 2003. Sensors 3, 544–554.
Wang, Z.Y., Liu, S.N., Wu, P., Cai, C.X., 2009. Analytical Chemistry 81, 1638–1645.
Wilson, R., Turner, A.P.F., 1992. Biosensors and Bioelectronics **7**, 165–185.
Wu, S., Ju, H.X., Liu, Y., 2007. Advanced Functional Materials 17, 585–592.
Yan, Y.M., Zheng, W., Su, L., Mao, L.Q., 2006. Advanced Materials 18, 2639–2643.
Yang, J., Zhang, R., Xu, Y., Xe, P., Fang, Y., 2008. Electrochemistry Communications 10, 1889–1892.
Yang, S.H., Kang, S.M., Lee, K.B., Chung, T.D., Lee, H., Choi, I.S., 2011. Journal of the American Chemical Society 133, 2795–2797.
Zhao, S., Zhang, K., Bai, Y., Yang, W.W., Sun, C.Q., 2006. Bioelectrochemistry 69, 158–163.
Zhang, M., He, X.W., Chen, L.X., Zhang, Y.K., 2010. Journal of Materials Chemistry 20, 10696–10704.
Zhang, X.L., Yu, M., Liu, J.H., Li, S.M., 2012. Chemical Communications 48, 8240–8242.
Zhou, W.H., Lu, C.H., Guo, X.C., Chen, F.R., Yang, H.H., Wang, X.R., 2010. Journal of Materials Chemistry 20, 880–883.